Chemical Engineering Science 206 (2019) 424–431

Contents lists available at ScienceDirect

Chemical Engineering Science

journal homepage: www.elsevier.com/locate/ces

Electrodeposited mesh-type dimensionally stable anode for oxygen evolution reaction in acidic and alkaline media

Ji Eun Park [a,b,1], Hyunjoon Lee [a,b,1], Seung-Hyeon Oh [c], Sun Young Kang [c], Insoo Choi [d], Yong-Hun Cho [c,*], Yung-Eun Sung [a,b,*]

[a] School of Chemical and Biological Engineering, Seoul National University, Seoul 08826, Republic of Korea
[b] Center for Nanoparticle Research, Institute for Basic Science (IBS), Seoul 08826, Republic of Korea
[c] Department of Chemical Engineering, Kangwon National University, Samcheok, Gangwon-do 25913, Republic of Korea
[d] Division of Energy Engineering, Kangwon National University, Samcheok, Gangwon-do 25913, Republic of Korea

HIGHLIGHTS

- A facile method for preparing a mesh-type dimensionally stable anode is proposed.
- Electrodeposition conditions were examined to attain uniform electrode.
- In acidic media, RuO_2/Ti electrode exhibited the highest performance.
- In alkaline media, DSA obtained with Ru:Ir ratio of 8:2 showed the highest activity.

GRAPHICAL ABSTRACT

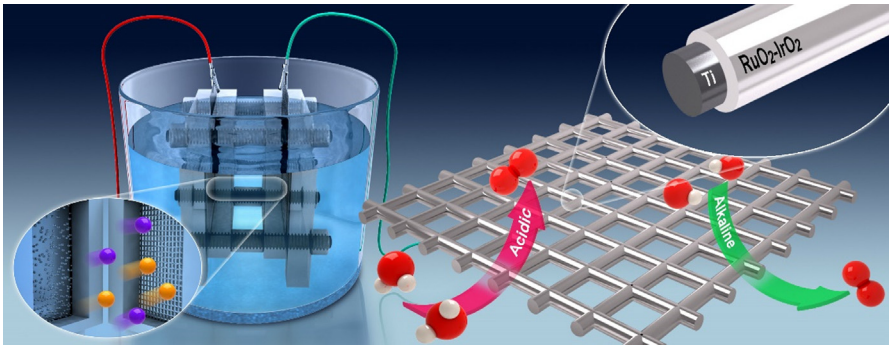

ARTICLE INFO

Article history:
Received 28 December 2018
Received in revised form 20 May 2019
Accepted 24 May 2019
Available online 30 May 2019

Keywords:
Dimensionally stable anode
Oxygen evolution electrode
Ruthenium oxide
Iridium oxide
Electrodeposition

ABSTRACT

A mesh-type dimensionally stable anode (DSA) consisting of ruthenium and iridium with low catalyst loading was prepared as an oxygen evolution reaction catalyst in acidic and alkaline media. The electrodeposition (ED) conditions, i.e., applied current density and total cycle number, and ED solutions with different precursor ratios of ruthenium to iridium are examined to fabricate various DSAs with a uniform thickness, and the effect of the iridium content on the catalytic activity is investigated. Among various DSA electrodes, the DSA electrode without iridium exhibits the highest activity and stability in the acidic medium owing to the high ratio of ruthenium. Conversely, the DSA electrode obtained using the ED solution with the ratio of 8:2 exhibits the highest performance in the alkaline medium. This is because the DSA electrode without iridium showed low stability, which is attributed to the dissolution of ruthenium oxide in the alkaline medium. In addition, two large-scale DSA electrodes optimized in the acidic and alkaline electrolytes show excellent performance, indicating the feasibility of the application of this electrode in practical electrolysis.

1. Introduction

Carbon emission from carbon-based fuels causes environmental problems. As a result, the interest in alternative energy sources has increased to solve these problems (Turner, 2004; Benson et al.,

* Corresponding authors at: Department of Chemical Engineering, Kangwon National University, Samcheok, Gangwon-do 25913, Republic of Korea (Y.-H. Cho), School of Chemical and Biological Engineering, Seoul National University, Seoul 08826, Republic of Korea (Y.-E. Sung).
E-mail addresses: yhun00@kangwon.ac.kr (Y.-H. Cho), ysung@snu.ac.kr (Y.-E. Sung).
[1] JEP and HL contributed equally to this work.

https://doi.org/10.1016/j.ces.2019.05.048
0009-2509/

2009; Cook et al., 2010; Suen et al., 2017). Currently, hydrogen is regarded as a new energy source to replace existing fossil fuels. Therefore, production and storage of hydrogen have become important technologies. Electrolysis of water using electricity or sunlight is the method that is being used for the environmentally benign production of hydrogen. However, hydrogen production through electrolysis is hindered by the kinetically slow oxygen evolution reaction (OER) at the anode (Suen et al., 2017; Gorlin and Jaramillo, 2010; Gong et al., 2013; Xia, 2016; Tahir et al., 2017). The hydrogen evolution reaction (HER) at the cathode is a two-electron reaction; however, the OER at the anode is a four-electron reaction with several steps, requiring higher energy to overcome the kinetic barrier. Therefore, it is important to develop an OER catalyst for the electrolysis with high efficiency. Ruthenium (Ru) oxide and iridium (Ir) oxide are considered highly efficient as OER catalysts (Suen et al., 2017; Tahir et al., 2017; Vuković, 1987; Fang and Liu, 2010; Tilley et al. 2010; Lee et al., 2012; Antolini, 2014; McCrory et al., 2015). However, these catalysts have some drawbacks, such as high cost owing to the use of platinum-group metal (PGM) and low stability in acidic and basic media. Thus, there arises a great need for the OER catalyst that contains low metal loading and also exhibits moderate catalytic activity and stability.

A dimensionally stable anode (DSA®) has been widely applied as an OER catalyst (Cipris and Pouli, 1976; Hu et al., 2004; Godwin and Lyons, 2013). The DSA consists of Ru, Ir, or their oxide coated on Ti or Ti oxide substrate (Godwin and Lyons, 2013). Various types of DSA with mixed oxides, such as RuO_2-TiO_2 (Takasu et al., 2010) and IrO_2-RuO_2-TiO_2 (Takasu et al., 2010; Yi et al., 2007), have been developed to improve the catalytic activity or stability toward water oxidation. In addition, diverse substrates, such as a rod, coil, and mesh, have been used to increase the utilization of the catalyst, thereby decreasing the catalyst loading. Choe et al., 2018 proposed iridium oxide (IrO_2)-coated Ti mesh as an oxygen evolution electrode for polymer electrolyte membrane water electrolysis (PEMWE). This mesh-type electrode exhibited high performance despite its low catalyst loading (0.4 mg cm^{-2}). This study demonstrated that the mesh-type electrode increased the utilization of the catalyst owing to the large surface area. Overall, the mesh-type DSA with mixed metal oxide is a good candidate to overcome the drawback of the Ru- or Ir-based OER catalyst.

Traditionally, the DSA electrode is made by thermal decomposition. However, the thermal decomposition method has several problems. The DSA electrode made by thermal decomposition always has some defects such as composition segregation and coarse particles, which are difficult to control (Xu et al., 2009). Also, it is difficult to make a precise composition coating and high heat is required. Therefore, in order to overcome these disadvantages, DSA electrodes in this study were fabricated by electrodeposition (ED) method. ED, the fabrication method that applies current or voltage to deposit metal onto a substrate by reducing the metal ions in the ED solution, has been used to prepare a uniform film on a mesh substrate.

The DSA has been prepared using ED method (Mussy et al., 2003; Devilliers and Mahe, 2010). Mussy et al. (2003) prepared Ti/TiO_2/Ir electrode as DSA electrode with iridium precursor solution. Also, Devilliers and Mahe (2010) synthesized lead dioxide (PbO_2) layer on Ti/TiO_2 substrate using lead precursor solution. These studies have been reported that the DSA electrodes prepared with ED method comprises one kind of metal or metal oxide. However, few studies regarding co-electrodeposition method, which is the electrodeposition using solution including two metal precursors (Jovic et al. 2006; Gui et al. 2015), have been conducted to fabricate the DSA electrode with two kinds of metal oxides. In this study, the DSA electrodes with different Ru to Ir ratios were fabricated by co-electrodeposition, which is easy to control the element ratio in DSA electrode. To the best of our knowledge, this is the first study applying the co-electrodeposition on DSA electrodes consisting of two metal oxides.

During ED, two conditions are required to develop a uniform deposit. First, cycling the on and off time of the applied current or voltage during ED (pulse ED) created a deposit with a uniform thickness. This was because the metal ions on the surface of the substrate could be replenished during the off time. In this study, pulse ED method was adopted for uniform coating instead of the general ED method. Additionally, a constant resistance in the entire electrode area is important to improve reproducibility. Thus, the distance between the working and counter electrodes should be maintained constant.

Here, the mesh-type DSAs; RuO_2/Ti and (RuO_2-IrO_2)/Ti electrodes were prepared as an oxygen evolution electrode in acidic and alkaline medium. The ED conditions, such as the applied current density and total cycle numbers, were optimized to obtain the RuO_2/Ti electrode with high film uniformity. In addition, the effect of catalyst composition in RuO_2-IrO_2/Ti on OER performance was investigated by varying the concentration of precursor solution. The catalytic activity of the prepared DSA was evaluated to achieve the optimal ratio of Ru to Ir in the electrode. Moreover, a large-scale DSA electrode was fabricated and evaluated as an oxygen evolution electrode.

2. Experimental

2.1. Fabrication of the DSA

To fabricate the RuO_2/Ti electrode, the pulse ED method was used on the Ti mesh substrate (100 mesh, Madelab Co., Republic of Korea) as shown in Fig. 1a. The precursor solution included

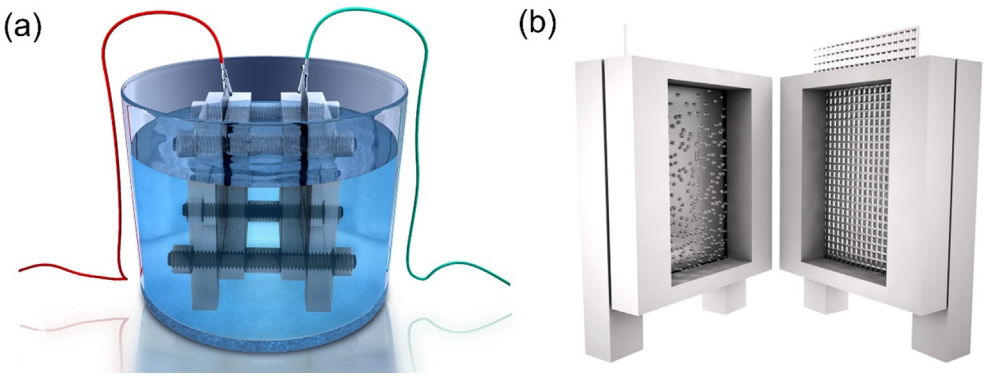

Fig. 1. (a) Schematic diagram of the fabrication method of the DSA electrode and (b) the template used in this study.

10 mM Ru chloride hydrate ($RuCl_3 \cdot xH_2O$, Sigma aldrich Co., USA), 100 mM potassium chloride (KCl, Samchun Chemicals Co., Republic of Korea), and distilled water. The three-electrode cell consisted of a working electrode (Ti mesh), counter electrode (Pt mesh, Alfa Aesar, USA), and reference electrode (Ag/AgCl electrode). To maintain the distance between the working and counter electrodes, a home-made Teflon template was used as shown in Fig. 2b. The applied current densities were 10, 20, 30, 40, and 80 mA cm^{-2} with an on/off time of 50/300 ms. The total cycle numbers varied with a constant charge applied to the electrode (80 k, 40 k, 26 k, 20 k, and 10 k for the applied current density of 10, 20, 30, 40, and 80 mA cm^{-2}, respectively). The exposed area to the electrolyte in the Teflon cell was 1 cm^2.

(RuO_2-IrO_2)/Ti electrodes were also prepared using a pulse co-electrodeposition method. The precursor solutions used in co-electrodeposition were composed of 100-mM potassium chloride, distilled water, and different ratios (8:2, 7:3, 6:4, 5:5, and 4:6) of Ru and Ir chloride hydrate ($IrCl_3 \cdot xH_2O$, Sigma aldrich Co., USA) with a constant total concentration of 10 mM. The applied current density was 20 mA cm^{-2}, and the on/off time was 50/300 ms. The total cycle number was 40 k cycles. The area of the DSA electrode was 1 cm^2.

To produce a large-scale electrode with the area of 5 cm^2, the total cycle number was increased because the total charge applied to the electrode is proportional to the electrode area. The total cycle numbers were 160 k, 240 k, and 400 k cycles. The applied current density was 20 mA cm^{-2}. Two types of DSA electrodes (the RuO_2/Ti and optimized (RuO_2-IrO_2)/Ti electrodes) were prepared to compare the catalytic activity.

2.2. Physical characterizations of the DSA

To investigate the morphology of the DSA, field-emission scanning electron microscope (FE-SEM; SUPRA 55VP, Carl Zeiss, Germany) was utilized. A focused-ion beam (FIB; Carl Zeiss, Germany) instrument was used to measure the uniformity and the thickness of the catalyst layer in the electrode. The elemental distribution was characterized using an energy dispersive X-ray spectrometer (EDS; Carl Zeiss, Germany). X-ray diffraction (XRD) spectra of the electrodes were obtained using an X-ray diffractometer (D/MAX-2500/PC, Rigaku Co., Japan). The surface composition of the DSA was measured using X-ray photoelectron spectroscopy (XPS; Sigma probe, Thermo, UK). The ratios of Ru to Ir in the DSA were obtained by inductively coupled plasma-mass spectroscopy (ICP-MS, NexION 350D, Perkin-Elmer, USA).

2.3. Electrochemical characterizations of the DSA

Electrochemical measurements were carried out using a potentiostat (PGSTAT302N; AUTOLAB) with a three-electrode electrochemical cell configuration at 25 °C in an electrolyte solution (0.1 M KOH or 0.1 M $HClO_4$) saturated with Ar. A Pt sheet electrode and a saturated calomel electrode (SCE) were used as the counter electrode and reference electrode, respectively. All SCE potentials in the acid and base were corrected to the reversible hydrogen electrode (RHE). The DSAs were used as the working electrodes. Cyclic voltammetry (CV) for the OER was conducted at a scan rate of 10 mV s^{-1}. The scan range of the CV was 1.2–1.65 V (vs. RHE). The potentials from the CV experiment were corrected with iR compensation. Also, stability test was conducted using chroamperometry conducted at 10 mA cm^{-2} for 7200 s. To compare the stability, commercial RuO_2 (Alfa Aesar Co., USA) was used as a standard material.

3. Results and discussion

3.1. Preparation and characterizations of the RuO_2/Ti electrode

The ED conditions, i.e., the applied current density and total cycle number, can affect the morphology of the deposited electrode. Therefore, the optimum deposition condition was derived by attaining the RuO_2 only; RuO_2/Ti electrode. Fig. 2 shows the SEM images of the pristine Ti mesh (Fig. 2a) and RuO_2/Ti electrodes (Fig. 2b–f), which were electrodeposited on the Ti mesh with different applied current densities of 10, 20, 30, 40, and 80 mA cm^{-2}. It was clearly seen that electrodeposited RuO_2 film covered the Ti mesh in all RuO_2/Ti electrodes. However, these electrodes exhibited different morphology based on their applied current density during ED. As shown in Fig. S1, the different voltage profiles were applied in the Ti mesh when the mesh was applied with a different current density. This is attributed to the different nucleation and growth rate according to current density during ED. When the current density was 10 mA cm^{-2}, low overpotential (Fig. S1a) and nucleation rate were observed, leading to insufficient amount of

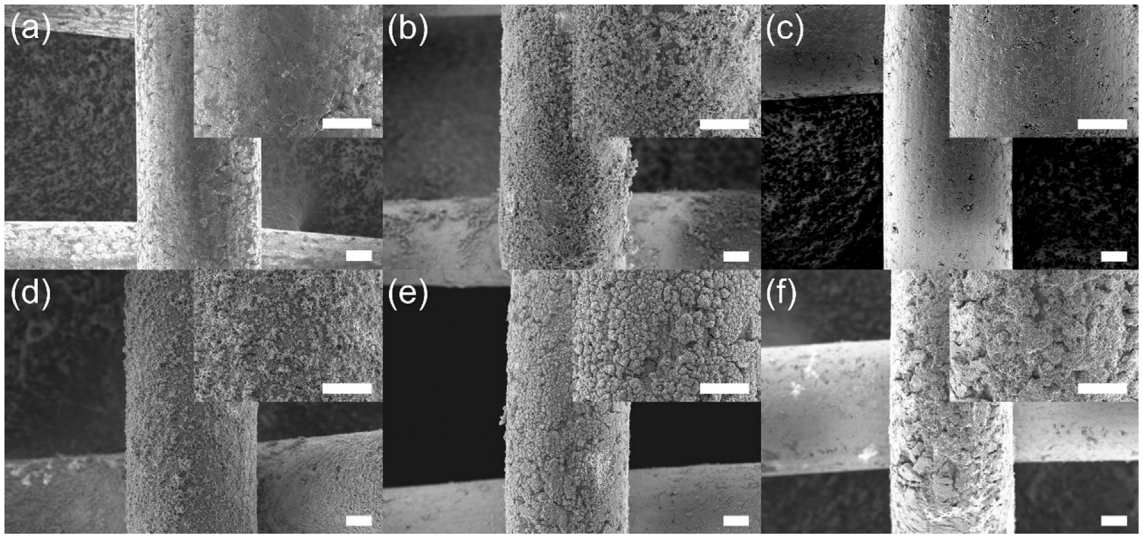

Fig. 2. FE-SEM images of the (a) pristine mesh and (b–f) DSA electrodes prepared using a precursor solution with a 10 mM Ru precursor. The applied current densities were (b) 10, (c) 20, (c) 30, (d) 40, and (e) 80 mA cm^{-2}. The scale bar was 20 μm.

nuclei to develop a uniform thin film (Fig. 2b) (Bicelli et al., 2008). The electrode obtained at the current density of 20 mA cm^{-2} exhibited an uniform RuO_2 thin film on the Ti mesh owing to the higher nucleation rate. However, much higher current density of 30, 40, and 80 mA cm^{-2} resulted in the formation of large particle, or dendrites. Therefore, the applied current density of 20 mA cm^{-2} is suitable for the preparation of thin RuO_2 film.

In addition, the RuO_2/Ti electrodes with different total cycle numbers were prepared to determine the effect of the total cycle number on the morphology of the electrode. The morphologies of the pristine Ti mesh and three RuO_2/Ti electrodes obtained using the total cycle numbers of 20 k, 40 k, and 160 k cycles are shown in Fig. S2. As these electrodes were fabricated at the optimal current density of 20 mA cm^{-2}, as discussed above, their morphologies showed the RuO_2 film covered the Ti mesh. For 20 k cycles, the electrode exhibited an uncovered RuO_2 film due to an insufficient amount of applied charge. With an increase from 20 k to 40 k, the thin RuO_2 film completely covered the Ti mesh, resulting in the fabrication of the RuO_2/Ti electrode. However, the total cycle number of 160 k cycles created an uneven RuO_2 film, which was attributed to an excessive charge. Thus, 40 k cycles is determined to be the optimal cycle number.

Fig. 3 shows the SEM images and EDS elemental mapping of the optimized RuO_2/Ti electrode obtained with the ED current density of 20 mA cm^{-2} and the total cycle number of 40 k cycles. This electrode exhibited an uniform RuO_2 film with a thickness of approximately 160 ± 30 nm (Fig. 3b). Also, EDS mapping showed that Ru and O were well distributed on the Ti mesh (Fig. 3c–e), which ensured the successful deposition of RuO_2 on Ti. In addition, the Ru $3d_{5/2}$ in XPS spectra showed that the peak position was approximately 280.7 eV (Fig. S3), which was consistent with the peak of RuO_2 (Han et al., 2010). In the XRD pattern (Fig. S4), diffraction peaks indexed to RuO_2 were not observed, and the intensity of the peaks of the Ti mesh was reduced, indicating that the prepared RuO_2 film covered the Ti mesh and had an amorphous phase.

3.2. Preparation and characterizations of the (RuO_2-IrO_2)/Ti electrodes

The (RuO_2-IrO_2)/Ti electrodes were fabricated using co-electrodeposition, which is ED using a precursor solution with two types of precursors (Ru and Ir). In co-electrodeposition, the ratio of the Ru to Ir precursors in the ED solution can influence the composition of the (RuO_2-IrO_2)/Ti electrodes. Thus, various uniform (RuO_2-IrO_2)/Ti electrodes with different compositions were prepared by modifying the ratio of Ru to Ir in the precursor solution (8:2, 7:3, 6:4, 5:5, and 4:6). The applied current density and total cycle number were 20 mA cm^{-2} and 40 k cycles, respectively, as previously optimized. The DSAs were denoted as A_B, where A_B represents the ratio of the Ru to Ir precursors in the ED solution.

Fig. 4 shows the FE-SEM images of the prepared (RuO_2-IrO_2)/Ti electrodes obtained with different ED solutions (8_2, 7_3, 6_4, 5_5, and 4_6). When prepared at the optimized current density of 20 mA cm^{-2}, all electrodes exhibited a similar morphology to that of the RuO_2/Ti electrode (10_0) that had a uniform thin film on the Ti mesh. Despite the different ED solution, the five different electrodes showed a similar voltage profile during ED, which is due to same nucleation and growth rate with constant current density of 20 mA cm^{-2} (Fig. S5). Fig. S6 shows the cross-sectional images of the (RuO_2-IrO_2)/Ti electrodes using an FIB-SEM analysis. All electrodes contained a RuO_2-IrO_2 film with a uniform thickness ranging from 160 ± 50 nm. EDS mapping (Fig. S7) showed that the materials covering the Ti mesh consisted of Ru, Ir, and O. Table 1 lists the composition (ratio of Ru to Ir) in the (RuO_2-IrO_2)/Ti electrodes measured using ICP-MS. The ratio of Ru to Ir increased with the increased ratio of the Ru precursor in the precursor solution. Therefore, the 8_2 electrode consisted of the highest RuO_2 ratio in the electrode.

XRD and XPS analyses were carried out to investigate the structural properties of the (RuO_2-IrO_2)/Ti electrodes and the oxidation state of Ru and Ir in the (RuO_2-IrO_2)/Ti electrodes. Fig. 5a shows the XRD spectra of the (RuO_2-IrO_2)/Ti electrodes (8_2, 7_3, 6_4, 5_5, and 4_6). However, in the XRD spectra, it was difficult to find a peak corresponding to Ru, RuO_2, Ir, or IrO_2. The XRD spectra of the (RuO_2-IrO_2)/Ti are almost same with the XRD spectrum of pristine Ti mesh. These results were similar to the XRD results of the RuO_2/Ti electrode shown in Fig. S4, indicating that prepared DSA has amorphous phase. Amorphous RuO_2 has been reported to exhibit improved OER performance compared to crystalline RuO_2 owing to its structural flexibility (Tsuji et al., 2011; Reier et al., 2012). While the crystalline RuO_2 can be deposited when using general ED method, the pulse ED method with longer off time

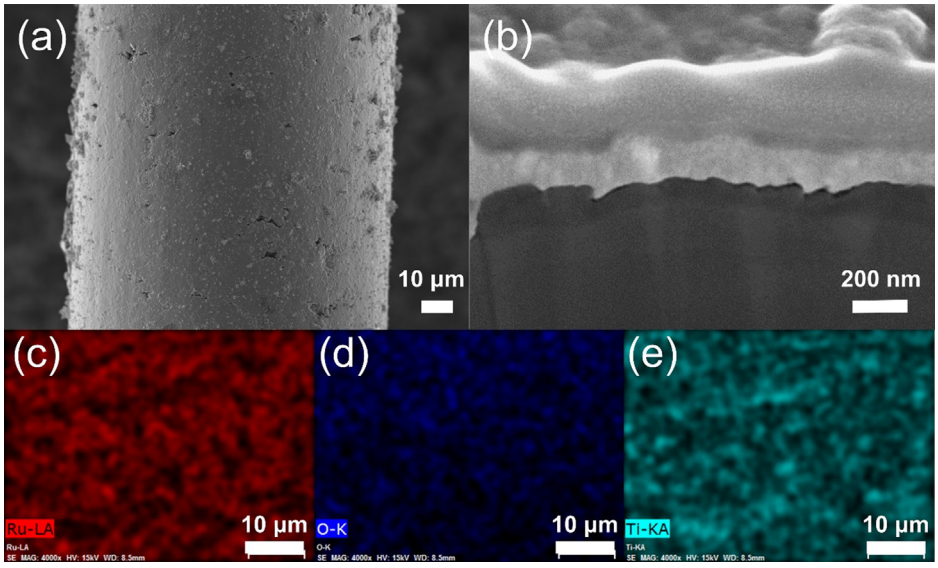

Fig. 3. (a) FE-SEM image of the RuO_2/Ti electrode. Image (b) shows the FIB-SEM cross-sectional view of the RuO_2/Ti electrode. Images (c–e) show the EDS elemental mapping of the large-scale RuO_2/Ti electrode: (c) Ru, (d) Ir, (e) O, and (f) Ti. The applied current density and total cycles were 20 mA cm^{-2} and 160 k cycles, respectively.

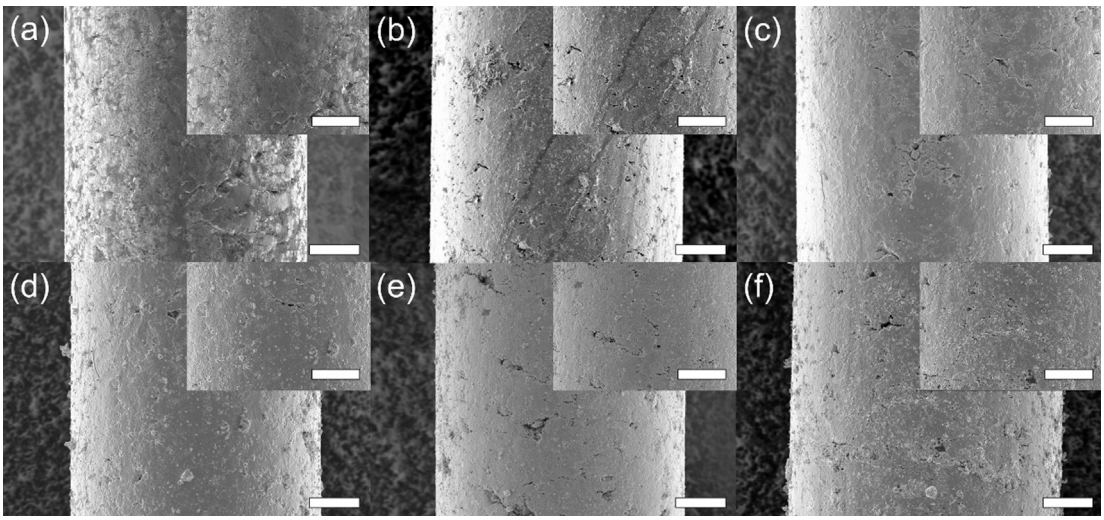

Fig. 4. FE-SEM images of the (a) pristine mesh and (b–f) DSA electrodes prepared with different ratios of Ru:Ir precursor solution: (b) 8_2, (c) 7_3, (d) 6_4, (e) 5_5, and (f) 4_6. The scale bar was 20 μm.

resulted in the fabrication of amorphous RuO_2. Therefore, the DSA prepared in this study were expected to have a higher activity than the OER electrode having crystallinity. The tiny peaks at around 42° in the XRD spectra of (RuO_2-IrO_2)/Ti indicate that the Ti mesh may be slightly oxidized due to ED. Fig. 5b–c shows the Ru 3d and Ir 4f XPS spectra of the (RuO_2-IrO_2)/Ti electrodes (8_2, 7_3, 6_4, 5_5, and 4_6). Each Ru 3d peak of the (RuO_2-IrO_2)/Ti electrodes appeared at approximately the same position, indicating that the Ru oxidation state of each electrode was the same. The position of each Ru $3d_{5/2}$ peak was approximately 280.7 eV, indicating that Ru was present as RuO_2, not as Ru metal. Each Ir 4f peak of the DSA also appeared at approximately the same position; thus, the Ir oxidation states of each electrode were the same. The position of each Ir $4f_{7/2}$ peak was shown at approximately 61.6 eV, which means that Ir was also present as IrO_2. It was confirmed that the (RuO_2-IrO_2)/Ti electrodes with the same oxidation state could be synthesized regardless of the ratio of Ru to Ir when they were fabricated using this ED method with the amorphous phase of RuO_2 and IrO_2. The surface composition of the (RuO_2-IrO_2)/Ti electrodes (8_2, 7_3, 6_4, 5_5, and 4_6) obtained from XPS is summarized in Table 2. The surface composition of the (RuO_2-IrO_2)/Ti electrodes was almost the same as the Ru and Ir ratios of the ED solution. As the Ru precursor ratio increased, the atomic percent of Ru increased, which is consistent with the ICP-MS result. Therefore, it was confirmed that the ED method proposed in this study can control the surface composition by controlling the ratios of Ru and Ir precursor.

3.3. Electrochemical characterizations of the DSA

The CV experiment results of the RuO_2/Ti electrode (10_0) and (RuO_2-IrO_2)/Ti electrodes with different Ru to Ir ratios in the alkaline and acidic electrolytes are shown in Fig. 6. To compare the performance of each electrode, the overpotential was calculated from the voltage at 10 mA cm^{-2}. In the acidic electrolyte (Fig. 6a), the overpotentials of 10_0, 8_2, 7_3, 6_4, 5_5, and 4_6 were 216 mV, 248 mV, 258 mV, 266 mV, 268 mV, and 277 mV, respectively. The results showed that the OER performance increased with an increasing RuO_2 ratio in acidic medium. Many researchers have concluded that RuO_2 is considered superior to IrO_2 in terms of the OER performance in both acidic and alkaline electrolyte because theoretical overpotential of RuO_2 for OER is lower than that of IrO_2 (Suen et al., 2017; Fabbri et al., 2014). Hence, as the ratio of RuO_2 increases, the OER performance increases and it has been reported that $RuIrO_x$ electrodes have a higher OER performance as the ratio of RuO_2 is higher (Audichon et al., 2014; Pham et al., 2015). For the alkaline electrolyte (Fig. 6b), this tendency is the same as that in the acidic electrolyte. These results are also due to the fact that RuO_2 is more active than IrO_2 in alkaline electrolyte (Suen et al., 2017; Cherevko et al., 2016). However, it was confirmed that 10_0 showed a poor performance. The overpotentials of the other electrodes were 303 mV, 310 mV, 358 mV, 398 mV, and 430 mV for 8_2, 7_3, 6_4, 5_5 and 4_6, respectively. These results were because the stability of 10_0 was degraded in the alkaline electrolyte. The RuO_2 has been reported to dissolve more rapidly in the alkaline electrolytes than the IrO_2 because, under anodic potential, the RuO_2 is more easily oxidized to the RuO_4 than the IrO_2 (Cherevko et al., 2016). In Fig. S8, 10_0 showed a stable performance in the acidic electrolyte; however, the performance decreased rapidly in only 3 cycles in the alkaline electrolyte. Conversely, 8_2 showed a stable OER performance in both acidic and alkaline electrolytes because the IrO_2 which is more stable than RuO_2 was mixed in the electrode. Ru and RuO_2 have a low stability despite the high OER performance. Therefore, to improve the stability of RuO_2, a mixture of RuO_2 and IrO_2 was proposed and the durability could be improved only by mixing a small amount of IrO_2 (Audichon et al., 2014). As a result of optimization, the RuO_2/Ti electrode (10_0) and (RuO_2-IrO_2)/Ti electrode (8_2) showed the highest performance in the acidic and alkaline electrolytes, respectively. For an objective performance evaluation, the OER performances of 10_0 in the acidic electrolyte and 8_2 in the alkaline electrolyte were compared to that of the Ru or Ir-based electrodes reported in other studies (McCrory et al., 2013,

Table 1
Ratios of Ru to Ir in the DSA electrodes measured using ICP-MS.

	8_2	7_3	6_4	5_5	4_6
Ru:Ir	3.4:1	2.3:1	1.9:1	1.4:1	0.5:1

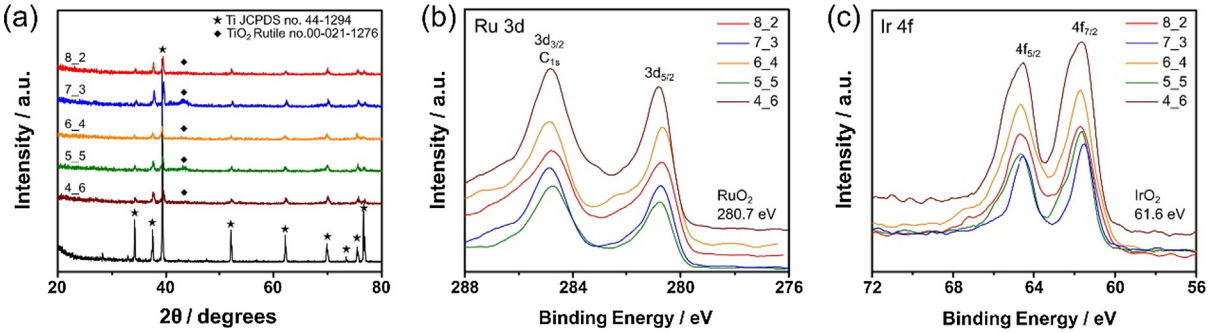

Fig. 5. (a) XRD patterns of the (RuO_2-IrO_2)/Ti electrodes and Ti mesh, and XPS spectra of (b) Ru 3d and (c) Ir 4f of the (RuO_2-IrO_2)/Ti electrodes.

Table 2
Atomic percent of the (RuO_2-IrO_2)/Ti electrodes measured using XPS.

	8_2	7_3	6_4	5_5	4_6
Ru Atomic percent (%)	82.5	77.8	56.8	53.8	37.0
Ir Atomic percent (%)	17.5	22.2	43.2	46.2	63.0

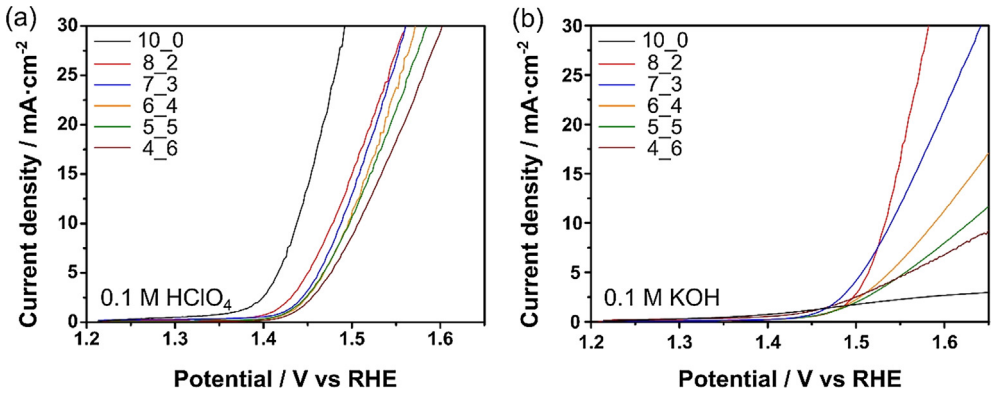

Fig. 6. Polarization curves of the RuO_2/Ti electrode (10_0) and (RuO_2-IrO_2)/Ti electrodes (8_2, 7_3, 6_4, 5_5, and 4_6) for the OER in (a) acidic and (b) alkaline electrolytes.

2015; Mattos-Costa et al., 1998; Zhao et al., 2013; Song and Hu, 2014; Ma et al., 2015; Salvatore et al., 2017; Browne et al., 2016). The results are listed in Table S1. The 10_0 and 8_2 electrodes showed excellent performance in spite of the small amount of metal loading (0.01 mg cm^{-2}), and the DSA electrode manufactured by this method was suitable as the OER electrode. Therefore, the DSA electrode fabricated in this study could be used in practical applications of electrolysis in the future.

3.4. Preparation and characterizations of large-scale DSA in acidic medium

Two large-scale DSA electrodes (10_0 and 8_2) were prepared to determine the feasibility of their application in a practical device. As the electrode area increased from 1 to 5 cm^2, a longer total cycle number was required to increase the applied charge. First, longer total cycle numbers (160 k, 240 k, and 400 k cycles) were examined to fabricate the 10_0 electrode with a uniform RuO_2-IrO_2 film. For 160 k cycles, the large-scale 10_0 electrode exhibited a uniform morphology. However, more cycles than 160 k resulted in the formation of dendrites on the electrode, as shown in Fig. S9. These results indicated that the optimal cycle number was 160 k. Figs. 7 and S10 show the morphology, EDS mapping, and photograph of the optimized large-scale 10_0 electrode. This electrode showed a similar morphology to that of the 10_0 electrode (Fig. 4) and a uniform RuO_2 film thickness of approximately 300 ± 50 nm. As shown Fig. S11, the entire area of 10_0 showed a uniform morphology. XRD showed a similar spectrum to that of the 10_0 electrode (Fig. S12a). Moreover, EDS mapping (Fig. 7c–e) and XPS spectra (Fig. S12b) also showed Ru, Ir, and O atoms distributed on the film. In addition to the 10_0 electrode, the large-scale 10_0 electrode exhibited an outstanding performance and stability in the acidic medium (210 mV at 10 mA·cm^{-2}), as shown in Figs. S13 and S14. As a result, it was confirmed that the large scale 10_0 has almost the same performance as the small scale 10_0, and that it does not change even when the scale of the DSA electrode is increased.

3.5. Preparation and characterizations of large-scale DSA in alkaline medium

Fig. 8 shows the FE-SEM and FIB-SEM images and EDS mapping of the large-scale 8_2 electrode. Large-scale 8_2 obtained using the cycle number of 160 k also contained a RuO_2-IrO_2 film with a thickness of approximately 320 ± 20 nm on the Ti mesh (Fig. S15), as the investigation of the total cycle numbers showed (Fig. S16). The peaks in the XRD results of the large-scale 8_2 electrode were smaller than those of the 8_2 electrode, indicating that a thicker RuO_2-IrO_2 film was formed on the Ti substrate (Fig. S17a). As shown in the EDS mapping (Fig. 8c-f) and XPS spectra (Fig. S17b–c), this electrode consisted of RuO_2 and IrO_2. The measured ratio of Ru to Ir using ICP-MS analysis was 3.2:1. This 8_2 electrode

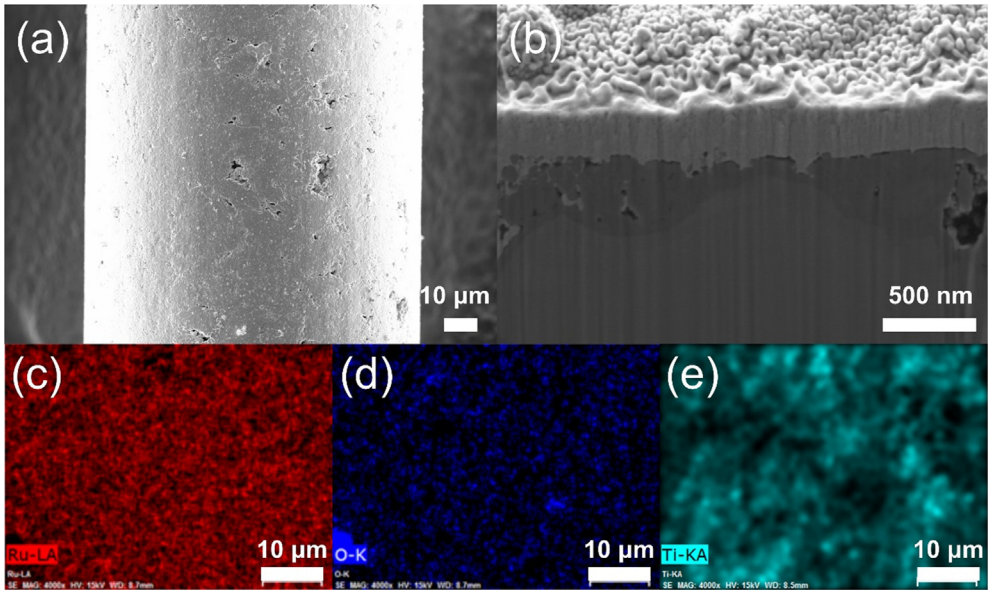

Fig. 7. (a) FE-SEM image of the large-scale 10_0 electrode. Image (b) shows the FIB-SEM cross-sectional view of the large-scale 10_0 electrode. Images (c–e) show the EDS elemental mapping of the large-scale 10_0 electrode: (c) Ru, (d) O, and (e) Ti. The applied current density and total cycles were 20 mA cm^{-2} and 160 k cycles, respectively.

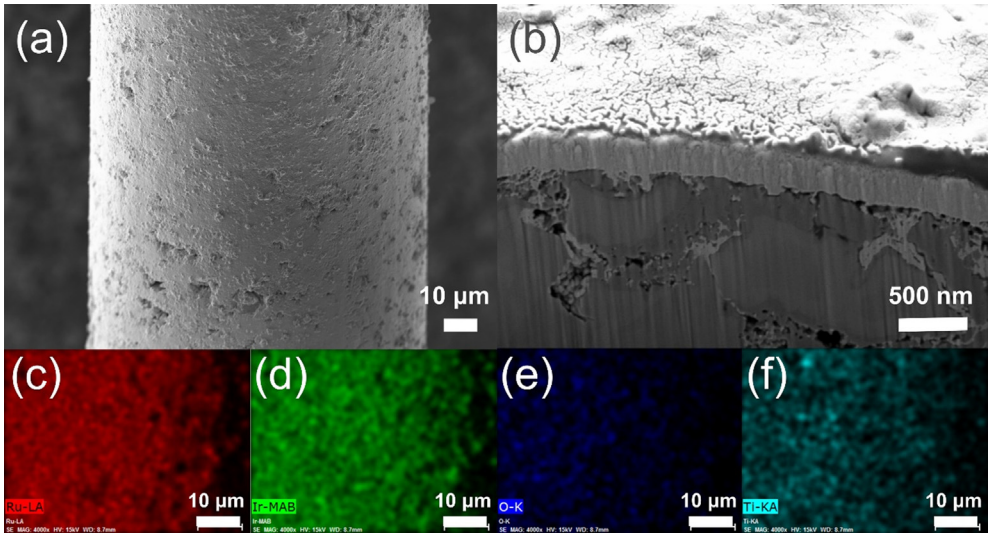

Fig. 8. (a) FE-SEM image of the large-scale 8_2 electrode. Image (b) shows the FIB-SEM cross-sectional view of the large-scale 8_2 electrode. Images (c–e) show the EDS elemental mapping of the large-scale 8_2 electrode: (c) Ru, (d) Ir, (e) O, and (f) Ti. The applied current density and total cycles were 20 mA cm^{-2} and 160 k cycles, respectively.

showed a high catalytic activity (303 mV at 10 mA·cm^{-2}) and stability in the acidic medium (Figs. S18 and S19). In conclusion, the performance of large scale 8_2 is almost the same as that of small scale 8_2 and it was confirmed that the same DSA electrode could be fabricated even when the scale of (RuO_2-TiO_2)/Ti electrode was increased. Therefore, the large-scale DSA electrode is a good candidate for the practical oxygen evolution electrode in both acidic and alkaline media.

4. Conclusions

DSA electrodes with a mesh substrate were synthesized as an oxygen evolution electrode using ED. The investigation of the ED conditions (applied current density and total cycle number) and precursor ratio in the ED solution determined the optimal ratio of Ru to Ir in the DSA electrode to investigate the effect of the Ir content on the catalytic activity and stability. The 10_0 electrode exhibited the highest activity in the acidic medium owing to the high amount of RuO_2. While the 10_0 electrode showed an unstable performance in the alkaline medium, which was attributed to the dissolution of RuO_2, the 8_2 electrode exhibited the highest performance. Therefore, a high amount of RuO_2 showed an increased catalytic activity in both acidic and alkaline media. However, the presence of Ir led to stability in the alkaline medium, preventing the dissolution of Ru. In addition, two large-scale DSA electrodes (10_0 in the acidic medium and 8_2 in the alkaline medium) showed outstanding performance. Therefore, this facile and reproducible method could be used to prepare a large-scale oxygen evolution electrode in acidic and alkaline electrolytes.

Declaration of Competing Interest

All authors must disclose any financial and personal relationships with other people or organizations that could inappropriately influence (bias) their work or state.

Acknowledgments

This work was supported by Project Code IBS-R006-A2 in Korea. Y.-H. C. acknowledges financial support from the Basic Science Research Program (2016R1D1A3B03934752) through the National Research Foundation of Korea (NRF), which is funded by the Ministry of Education. This research was also supported by Korea Electric Power Corporation (Grant number: R16VA08). This study was supported by 2018 Research Grant (PoINT) from Kangwon National University.

Appendix A. Supplementary material

Supplementary data to this article can be found online at https://doi.org/10.1016/j.ces.2019.05.048.

References

Antolini, E., 2014. Iridium as catalyst and cocatalyst for oxygen evolution/reduction in acidic polymer electrolyte membrane electrolyzers and fuel cells. ACS Catal. 4, 1426–1440.

Audichon, T., Mayousse, E., Morisset, S., Morais, C., Comminges, C., Napporn, T.W., Kokoh, K.B., 2014. Electroactivity of RuO_2–IrO_2 mixed nanocatalysts toward the oxygen evolution reaction in a water electrolyzer supplied by a solar profile. Int. J. Hydrogen Energy 39, 16785–16796.

Benson, E.E., Kubiak, C.P., Sathrum, A.J., Smieja, J.M., 2009. Electrocatalytic and homogeneous approaches to conversion of CO2 to liquid fuels. Chem. Soc. Rev. 38, 89–99.

Bicelli, L.P., Bozzini, B., Mele, C., 2008. A review of nanostructural aspects of metal electrodeposition. Int. J. Electrochem. Sci. 3, 356–408.

Browne, M.P., Nolan, H., Twamley, B., Duesberg, G.S., Colavita, P.E., Lyons, M.E.G., 2016. Thermally prepared Mn_2O_3/RuO_2/Ru thin films as highly active catalysts for the oxygen evolution reaction in alkaline media. ChemElectroChem 3, 1847–1855.

Cherevko, S., Geiger, S., Kasian, O., Kulyk, N., Grote, J., Savan, A., Shrestha, B.R., Merzlikin, S., Breitbach, B., Ludwig, A., Mayrhofer, K.J.J., 2016. Oxygen and hydrogen evolution reactions on Ru, RuO_2, Ir, and IrO_2 thin film electrodes in acidic and alkaline electrolytes: a comprarative study on activity and stability. Catal. Today 262, 170–180.

Choe, S., Lee, B.S., Cho, M.K., Kim, H.J., Henkensmeier, D., Yoo, S.J., Kim, J.Y., Lee, S.Y., Park, H.S., Jang, J.H., 2018. Electrodeposited IrO_2/Ti electrodes as durable and cost-effective anodes in high-temperature polymer-membrane-electrolyte water electrolyzers. Appl. Catal. B-Environ. 226, 289–294.

Cipris, D., Pouli, D., 1976. Oxygen evolution on dimensionally stable anode materials. J. Electroanal. Chem. Interfacial Electrochem. 73, 125–128.

Cook, T.R., Dogutan, D.K., Reece, S.Y., Surendranath, Y., Teets, T.S., Nocera, D.G., 2010. Solar energy supply and storage for the legacy and nonlegacy worlds. Chem. Rev. 110, 6474–6502.

Devilliers, D., Mahe, E., 2010. Modified titanium electrodes: application to Ti/TiO_2/PhO_2 dimensionally stable anodes. Electrochim. Acta 55, 8207–8214.

Fabbri, E., Habereder, A., Waltar, K., Kotz, R., Schmidt, T.J., 2014. Developments and perspectives of oxide-based catalysts for the oxygen evolution reaction. Catal. Sci. Technol. 4, 3800–3821.

Fang, Y.-H., Liu, Z.-P., 2010. Mechanism and Tafel lines of electro-oxidation of water to oxygen on RuO_2(110). J. Am. Chem. Soc. 132, 18214–18222.

Godwin, I., Lyons, M.E.G., 2013. Dimensionally stable anodes (DSA®) for electrochemical water splitting: redox properties, OER kinetics and mechanism at RuO_2/NiO modified electrodes in aqueous base. ECS Trans. 53, 21–31.

Gong, M., Li, Y., Wang, H., Liang, Y., Wu, J.Z., Zhou, J., Wang, J., Regier, T., Wei, F., Dai, H., 2013. An advanced Ni-Fe layered double hydroxide electrocatalyst for water oxidation. J. Am. Chem. Soc. 135, 8452–8455.

Gorlin, Y., Jaramillo, T.F., 2010. A bifunctional nonprecious metal catalyst for oxygen reduction and water oxidation. J. Am. Chem. Soc. 132, 13612–13614.

Gui, Z., Gillette, E., Duay, J., Hu, J., Kim, N., Lee, S.B., 2015. Co-electrodeposition of RuO_2-MnO_2 nanowires and the contribution of RuO_2 to the capacitance increase. Phys. Chem. Chem. Phys. 17, 15173–15180.

Han, J.H., Lee, S.W., Kim, S.K., Han, S., Hwang, C.S., Dussarrat, C., Gatineau, J., 2010. Growth of RuO_2 thin films by pulsed-chemical vapor deposition using RuO_4 precursor and 5% H_2 reduction gas. Chem. Mater. 22, 5700–5706.

Hu, J.-M., Zhang, J.-Q., Cao, C.-N., 2004. Oxygen evolution reaction on IrO_2-based DSA® type electrodes: kinetics analysis of Tafel lines and EIS. Int. J. Hydrogen Energy 29, 791–797.

Jovic, V.D., Jovic, B.M., Pavlovic, M.G., 2006. Electrodeposition of Ni, Co and Ni-Co alloy powders. Electrochem. Acta 51, 5468–5477.

Lee, Y., Suntivich, J., May, K.J., Perry, E.E., Shao-Horn, Y., 2012. Synthesis and activities of rutile IrO_2 and RuO_2 nanoparticles for oxygen evolution in acid and alkaline solutions. J. Phys Chem Lett. 3, 399–404.

Ma, W., Ma, R., Wang, C., Liang, J., Liu, X., Zhou, K., Sasaki, T., 2015. A superlattice of alternately stacked Ni–Fe hydroxide nanosheets and graphene for efficient splitting of water. ACS Nano 9, 1977–1984.

Mattos-Costa, F.I., de Lima-Neto, P., Machado, S.A.S., Avaca, L.A., 1998. Characterisation of surfaces modified by sol-gel derived $Ru_xIr_{1-x}O_2$ coatings for oxygen evolution in acid medium. Electrochim. Acta 44, 1515–1523.

McCrory, C.C.L., Jung, S., Peters, J.C., Jaramillo, J.C., 2013. Benchmarking heterogeneous electrocatalysts for the oxygen evolution reaction. J. Am. Chem. Soc. 135, 16977–16987.

McCrory, C.C., Jung, S., Ferrer, I.M., Chatman, S.M., Peters, J.C., Jaramillo, T.F., 2015. Benchmarking hydrogen evolving reaction and oxygen evolving reaction electrocatalysts for solar water splitting devices. J. Am. Chem. Soc. 137, 4347–4357.

Mussy, J.-P.G., Macpherson, J.V., Delplancke, J.-L., 2003. Characterisation and behaviour of Ti/TiO_2/noble metal anodes. Electrochim. Acta 48, 1131–1141.

Pham, H.H., Nguyen, N.P., Do, C.L., Le, B.T., 2015. Nanosized $Ir_xRu_{1-x}O_2$ electrocatalysts for oxygen evolution reaction in proton exchange membrane water electrolyzer. Adv. Nat. Sci. Nanosci. Nanotechnol. 6, 025015.

Reier, T., Oezaslan, M., Strasser, P., 2012. Electrocatalytic oxygen evolution reaction (OER) on Ru, Ir, and Pt catalysts: a comparative study of nanoparticles and bulk materials. ACS Catal. 2, 1765–1772.

Salvatore, D.A., Pena, B., Dettelbach, K.E., Berlinguette, C.P., 2017. Photodeposited ruthenium dioxide films for oxygen evolution reaction electrocatalysis. J. Mater. Chem. A 5, 1575–1580.

Song, F., Hu, X., 2014. Exfoliation of layered double hydroxides for enhanced oxygen evolution catalysis. Nat. Commun. 5, 4477.

Suen, N.-T., Hung, S.-F., Quan, Q., Zhang, N., Xu, Y.-J., Chen, H.M., 2017. Electrocatalysis for the oxygen evolution reaction: recent development and future perspectives. Chem. Soc. Rev. 46, 337–365.

Tahir, M., Pan, L., Idrees, F., Zhang, X., Wang, L., Zou, J.-J., Wang, Z.L., 2017. Electrocatalytic oxygen evolution reaction for energy conversion and storage: a comprehensive review. Nano Energy 37, 136–157.

Takasu, Y., Sugimoto, W., Nishiki, Y., Nakamatsu, S., 2010. Structural analyses of RuO_2–TiO_2/Ti and IrO_2–RuO_2–TiO_2/Ti anodes used in industrial chlor-alkali membrane processes. J. Appl. Electrochem. 40, 1789–1795.

Tilley, S.D., Cornuz, M., Sivula, K., Gratzel, M., 2010. Light-induced water splitting with hematite: improved nanostructure and iridium oxide catalysis. Angew. Chem. Int. Ed. Engl. 49, 6405–6408.

Tsuji, E., Imanishi, A., Fukui, K.-I., Nakato, Y., 2011. Electrocatalytic activity of amorphous RuO_2 electrode for oxygen evolution in an aqueous solution. Electrochim. Acta 56, 2009–2016.

Turner, J.A., 2004. Sustainable hydrogen production. Science 305, 972–974.

Vuković, M., 1987. Oxygen evolution reaction on thermally treated iridium oxide films. J. Appl. Electrochem. 17, 737–745.

Xia, Z., 2016. Hydrogen evolution: guiding principles. Nat. Energy 1, 16155.

Xu, L., Xin, Y., Wang, J., 2009. A comparative study on IrO_2-Ta_2O_5 coated titanium electrodes prepared with different methods. Electrochim. Acta 54, 1820–1825.

Yi, Z., Kangning, C., Wei, W., Wang, J., Lee, S., 2007. Effect of IrO_2 loading on RuO_2–IrO_2–TiO_2 anodes: a study of microstructure and working life for the chlorine evolution reaction. Ceram. Int. 33, 1087–1091.

Zhao, Y., Nakamura, R., Kamiya, K., Nakanishi, S., Hashimoto, K., 2013. Nitrogen-doped carbon nanomaterials as non-metal electrocatalysts for water oxidation. Nat. Commun. 4, 2390.